Geophysical Journal International

Geophys. J. Int. (2024) **237,** 364–377
Advance Access publication 2024 February 05
GJI Geodynamics and Tectonics

https://doi.org/10.1093/gji/ggae047

Toroidal mantle flow beneath the NE termination of the Kuril–Kamchatka subduction zone from seismic anisotropy

Ayoub Kaviani [1], Georg Rümpker [1,2], Christoph Sens-Schönfelder [3], Abolfazl Komeazi [1] and Nikolai Shapiro [4]

[1] *Institute of Geosciences, Goethe University Frankfurt, Frankfurt D-*60438*, Germany, E-mail: kaviani@geophysik.uni-frankfurt.de*
[2] *Frankfurt Institute for Advanced Studies, Frankfurt D-*60438*, Germany*
[3] *GFZ German Research Centre for Geosciences, Potsdam D-*14473*, Germany*
[4] *Institut des Sciences de la Terre (ISTERRE), UMR CNRS* 5375*, Université Grenoble-Alpes, Grenoble CS* 40700 38058 *Cedex* 9*, France*

Accepted 2024 February 3. Received 2024 January 21; in original form 2023 August 21

SUMMARY

This study presents the findings of a splitting analysis conducted on core-refracted teleseismic shear waves (*SKS*, *SKKS* and *PKS*, called together as *XKS*) and local shear waves, obtained from a dense seismological network spanning the Kamchatka Peninsula. The objective of the study is to examine the pattern of mantle flow beneath the study area through the investigation of seismic anisotropy. The peninsula is situated at the northeastern end of the Kuril–Kamchatka subduction zone, where the Kuril trench intersects with the western boundary of the Aleutian trench. The data set utilized in this study comprises waveform data from a dense network of seismic stations (99 broad-band and short-period stations for the local shear wave splitting analysis and 69 broad-band stations for the *SKS* splitting analysis). The seismograms were downloaded from publicly available data repositories including the IRIS Data Management Center and the GFZ Data Services (GEOFON program). The dense station coverage allows us to investigate the lateral variations in anisotropy, providing insights into the flow patterns within the mantle. The processing of the combined data sets of local shear wave and teleseismic *XKS* waves allowed us to partially decipher the source of anisotropy in the mantle. Small delay (splitting) times (∼0.35 s) observed from the local-*S* data suggest that anisotropy in the mantle wedge is relatively weak with lateral variations. Larger splitting times (∼1.1 s) observed for the *XKS* waves relative to local *S* suggest that the main part of splitting on the *XKS* waves occurs in the subslab mantle. On the other hand, the rotational pattern of seismic anisotropy observed by both the local *S* and *XKS* waves suggests the presence of a toroidal flow at the NE edge of the subducting slab, which affects both the mantle wedge and subslab mantle. For the regions away from the edge of the slab, the mantle flow seems to be governed mainly by the drag of the lithospheric plate over the underlying asthenosphere.

Key words: Seismic anisotropy; Kinematics of crustal and mantle deformation; Subduction zone processes.

1 INTRODUCTION

Probing the mantle flow field in subduction zones is essential for a better understanding of mantle dynamics and comprehending the relationship between tectonic activities at the surface and mantle deformation associated with plate convergence. The interaction between the subducting plate and surrounding mantle can lead to specific mantle flow patterns depending on parameters such as plate geometry, subduction angle and convergence velocity (e.g. Long 2013). The simplest mode of flow in the mantle wedge above the subducting slab is a 2-D corner flow induced by shear coupling between the downgoing slab and the overlying mantle (e.g. van Keken 2003; Long & Wirth 2013). However, this simple 2-D flow can be affected by 3-D variations induced by trench migration, proximity to slab edge and along-strike variation in the slab geometry (Kneller & van Keken 2008; Kenyon & Wada 2022). The subslab asthenospheric flow is generally governed by the plate motion but it can also be affected by the slab retreat and angle of subduction (e.g. Long & Silver 2009; Zhao *et al.* 2023).

The study of seismic anisotropy provides a unique tool to characterize the mantle flow field (e.g. Silver 1996; Savage 1999). Seismic anisotropy in the upper mantle is generally considered the consequence of the development of lattice-preferred orientation (LPO) in olivine minerals (Zhang & Karato 1995), as the most abundant

mineral in the upper mantle (Ben Ismail & Mainprice 1998). In a subduction setting, seismic anisotropy can be developed in the upper plate, the mantle wedge, the subducting plate and the subslab mantle (Silver & Savage 1994).

Seismic anisotropy can be quantified by shear wave splitting (SWS) analysis (Silver & Chan 1991; Silver & Savage 1994; Silver 1996; Savage 1999). SWS analysis is based on the phenomenon that, by propagating through an anisotropic medium, a shear wave splits into two components (fast and slow) with orthogonal polarizations that travel at different speeds. Therefore, a splitting time (δt) is accumulated between the fast and slow shear waves along the ray path as a function of the strength and thickness of the layer of anisotropy. The polarization direction of the fast shear wave (φ) provides information about the orientation of seismic anisotropy (e.g. Silver & Chan 1991). Splitting analysis of a combined data set of shear waves originating from local events and core-refracted teleseismic *S* waves (*PKS*, *SKKS* and *SKS*, collectively called *XKS* henceforth) provides the opportunity to investigate seismic anisotropy in the subduction zone in more detail (e.g. Long & Silver 2009; Long & Wirth 2013; Wölbern *et al.* 2014; Reiss *et al.* 2018).

Mantle wedge SWS patterns in subduction zones worldwide are very variable, with large variations both in average splitting times and fast directions (e.g. Long & Silver 2008; Long & Wirth 2013). Globally, local splitting studies report the most common splitting patterns with an arc-parallel trend in the forearc that transitions to arc-perpendicular directions in the backarc. The arc-parallel direction is usually attributed to B-type LPO fabric developed by the corner flow in the colder and hydrated portion of the mantle wedge (Kneller *et al.* 2005; Karato *et al.* 2008), while the arc-perpendicular direction is attributed to the slab-entrained asthenospheric flow both in the mantle wedge and beneath the subducting plate (Long & Wirth 2013; Kong *et al.* 2020; Richards *et al.* 2021;). However, a recent SWS analysis in the forearc region of the central Andean margin (Wölbern *et al.* 2014; Reiss *et al.* 2018) does not show any evidence for arc-parallel mantle flow.

This study aims at examining the pattern of the mantle flow beneath the Kuril–Kamchatka subduction zone (KSZ) by investigating seismic anisotropy using shear wave data both from local and teleseismic events. The KSZ is a seismically active and dynamic convergent tectonic boundary in Northeast Eurasia, where the Pacific Plate is being subducted beneath the Okhotsk Plate along the Kuril Islands and the Kamchatka Peninsula (Figs 1 and 2a). The subduction zone extends for >2000 km from the southern tip of the Kamchatka Peninsula to Hokkaido, Japan and has been the site of many large earthquakes and volcanic eruptions (e.g. Senyukov 2013; Senyukov *et al.* 2015). In addition to the relatively fast plate convergence rate ($\sim$8 cm yr^{-1}, Steblov *et al.* 2010; Kreemer *et al.* 2014), tomography images also suggest a slab termination beneath the northern Kamchatka Peninsula (Levin *et al.* 2002; Koulakov *et al.* 2011, 2020; Koulakov 2022). The focus of the current study is on the Central Kamchatka Depression (CKD), where the Klyuchevskoy Volcanic Group (KVG) consisting of a cluster of several volcanoes, including Klyuchevskoy, Bezymianny and Tolbachik is located. All of these volcanoes are stratovolcanoes, which are characterized by their steep sides and periodic explosive eruptions (e.g. Ponomareva *et al.* 2007; Fedotov *et al.* 2010). The CKD is bounded by the tectonic mountain ranges Tumrok and Kumroch ranges to the east and Sredinny Range to the west. To the south, Pleistocene and Holocene volcanoes form the East Volcanic Front in the arc region of the Kuril–Kamchatka subduction (e.g. Portnyagin *et al.* 2005).

The slab model reconstructed from the track of slab seismicity and seismic images (Hayes 2018) shows that the upper boundary of the subducting Pacific Plate is located at $\sim$150 km beneath the KVG. The potential gap between the southern (Kuril–Kamchatka) and northern (Aleutian) segments of the Pacific slab provides a window that can allow flow from the subslab mantle into the mantle wedge and also facilitate the occurrence of toroidal flow at the slab edge (e.g. Faccenda & Capitanio 2013). This specific configuration makes the Kamchatka subduction zone an interesting region to study the pattern of mantle flow in the case of slab termination. Furthermore, the relatively high seismic activity at this subduction zone provides considerable seismic data from local earthquakes to study mantle wedge seismic anisotropy.

The data from the dense Klyuchevskoy Volcanic Group experiment (KISS) seismic network (Shapiro *et al.* 2021; Network DOI:10.14470/K47560642124) and previous temporary deployments and long-term observations at the two permanent stations provide a unique opportunity for a high-resolution study of seismic anisotropy beneath the Kamchatka peninsula. By combining data from subduction events with teleseismic shear waves ascending from the deep mantle, one can better infer the source depth of seismic anisotropy in a subduction zone, which in turn allows examining the interaction between the flow in the mantle wedge and subslab mantle (e.g. Long & Silver 2009; Wölbern *et al.* 2014; Reiss *et al.* 2018).

2 DATA AND METHOD

The main data set used in this study was collected from a large-scale temporary seismic deployment named KISS (Fig. 2) consisting of 79 stations that operated between 2015 September and 2016 May to cover the entire area of the KVG (Shapiro *et al.* 2017). In order to improve the resolution and extend the data coverage to a broader region surrounding the Kamchatka peninsula, we also included data from two permanent stations (IU.PET and IU.MA2, from 2010 April to 2020 September, Network DOI:10.7914/SN/IU) and 18 temporary stations from two previous deployments (YC: 2007–2010 July, Network DOI:10.7914/SN/YC_2006, and XJ: 1998–1999 August, Network DOI:10.7914/SN/XJ_1998z).

For the local SWS analysis, we used waveform data from 99 broad-band and short-period stations for earthquakes that occurred in the mantle wedge or on the upper surface of the subducting slab (Fig. 3a). The broad-band stations were equipped with either a Nanometrics Trillium Compact sensor (>60 s) or a Güralp 6T sensor (standard response of 30 s to 100 Hz). The short-period stations were equipped with Mark L-4C-3D 3-component 1-Hz geophones. We used a combined catalog of local events requested from the Kamchatka Branch of the Geophysical Survey of the Russian Academy of Sciences and USGS (NEIC). For the time during the KISS experiment, we also included local events from the catalogue published by Senyukov et al. (2024) based on the data set from the KISS network. For each individual station, only events giving an *S*-wave ray path with an incidence angle less than 35° are used. Waveform data were filtered in the frequency range 0.20–1.50 Hz in order to remove high- and low-frequency noise. The direct *S*-wave window is selected manually on each seismogram and the windowed waveforms with a pre-phase signal-to-noise ratio (SNR) of larger than 1.5 are used for splitting analysis. The splitting parameters were obtained using both the eigenvector analysis (Silver & Chan 1991) and cross-correlation calculation (Bowman & Ando 1987) of horizontal components of the shear wave. In both methods, the splitting parameters can be estimated independent of the knowledge about the initial polarization of the shear waveform. We finally report

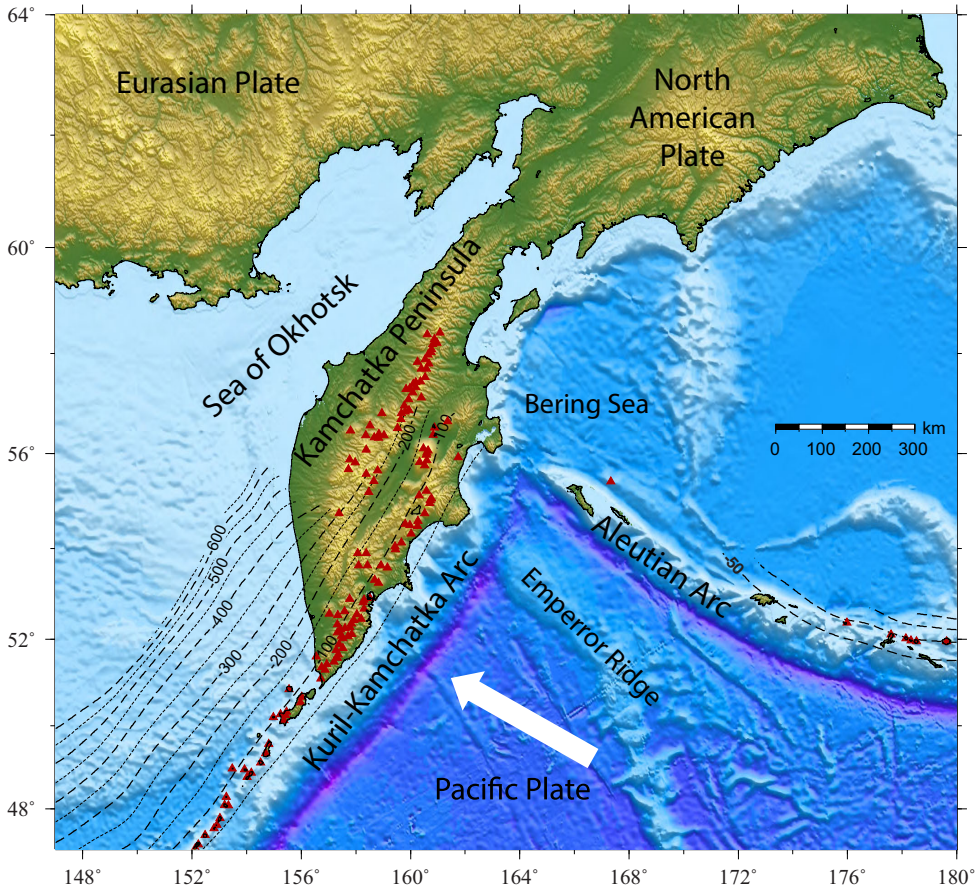

Figure 1. Geological framework of the study area with two subduction zones involved: the Kuril–Kamchatka slab subducting beneath the Eurasian Plate and Aleutian slab subducting beneath the North American Plate. The contours indicate the depth to the upper surface of the subducting slabs (Hayes 2018). The triangles mark the location of quaternary volcanoes from the Global Volcanism Program, 2023. Volcanoes of the World (v. 5.1.5; 2023 December 15). Distributed by Smithsonian Institution, compiled by Venzke, E. https://doi.org/10.5479/si.GVP.VOTW5-2023.5.1. The thick arrow indicates the direction of the motion of the Pacific Plate in the No-Net-Rotation reference frame (Kreemer *et al.* 2014).

the splitting parameters obtained from the eigenvector analysis as a standard approach for local-*S* splitting analysis (Silver & Chan 1991). Each splitting measurement is also visually controlled for its quality and reliability. The first criterion is the sharpness of the *S* wave selected for the processing. This is quantified according to the pre-phase SNR. Any measurement with a waveform of an SNR < 2 is taken as a 'fair' measurement. The second criterion is how well the estimation of the splitting parameters is constrained on the eigenvalue energy diagram. The third important criterion is how well the estimated parameters can remove the energy on the tangential component of the seismogram. In the end, the measurements are classified as 'good', 'fair' or 'poor'. In the case of a large discrepancy ($>20^\circ$ for the fast polarization direction, FPD or > 0.15 s for the splitting time) between the estimates of splitting parameters from the two methods (eigenvector analysis and correlation), the measurement is considered as 'poor', and is not used. An example of local splitting analysis is shown in Fig. 4(a). Finally, we report 916 individual measurements in categories 'good' and 'fair' (Table S1, Supporting Information) and use them for the subsequent synthesis and interpretations.

For the *XKS* splitting analysis, waveform data were collected at 69 broad-band stations from 302 teleseismic events that occurred in the epicentral distance range 87°–144° (Fig. 3b) and with magnitudes $M_w > 6.2$ giving a total number of 2060 seismograms. Splitting analysis is performed using both the *T*-component minimization (Silver & Chan 1991) and cross-correlation (Bowman & Ando 1987) methods. Reiss and Rümpker, (2017) introduced an approach of joint splitting analysis of shear waves to obtain mean values of splitting parameters for each station. However, in our study, we analyse each waveform separately, since we aim at projecting the individual measurements to different depths in order to examine the depth and lateral distribution of anisotropy. *XKS* seismograms are filtered in the range of 0.02–0.4 Hz. A semi-automatic windowing approach is applied to measure splitting parameters, in which the best window is searched automatically within a time window defined manually around the desired *XKS* phase. The criteria for the best window are SNR (>1.5), the sharpness of the *XKS* waveform, and the ellipticity of the horizontal component particle motion. For the final best window, we first perform the cross-correlation analysis to estimate the initial polarization of the *XKS* phase. If the difference between the geometrical backazimuth and the estimated initial polarization direction is larger than 20°, the waveform is not used. Finally, a quality value ('good', 'fair' and 'poor') is assigned to each measurement according to the similarity of the estimates from the two methods, linearity of the particle motion after removal of the effect of splitting, and the maximum cross-correlation (at least 0.90) between the fast and slow components (e.g. Kaviani *et al.* 2013). Like the local-*S* splitting analysis, we also compare the values of the splitting parameters estimated using the *T*-component minimization and cross-correlation methods and discard the measurement in the

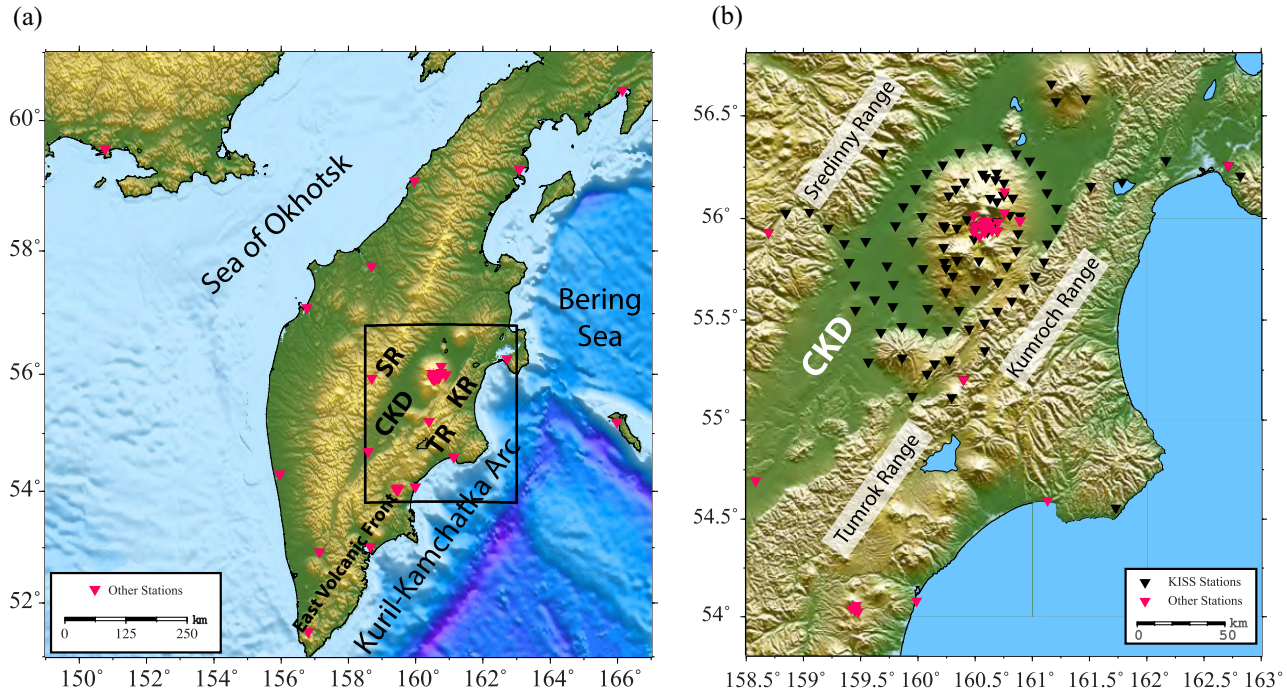

Figure 2. Locations of the stations used in this study: (a) a wide view over the Kamchatka Peninsula showing the location of stations (purple triangles) from previous deployments. CKD: Central Kamchatka Depression; SR: Sredinny Range; KR: Kumroch Range; TR: Tumrok Range. (b) A zoomed view over the CKD and the KVG to highlight the dense and uniform distribution of the KISS stations (black triangles).

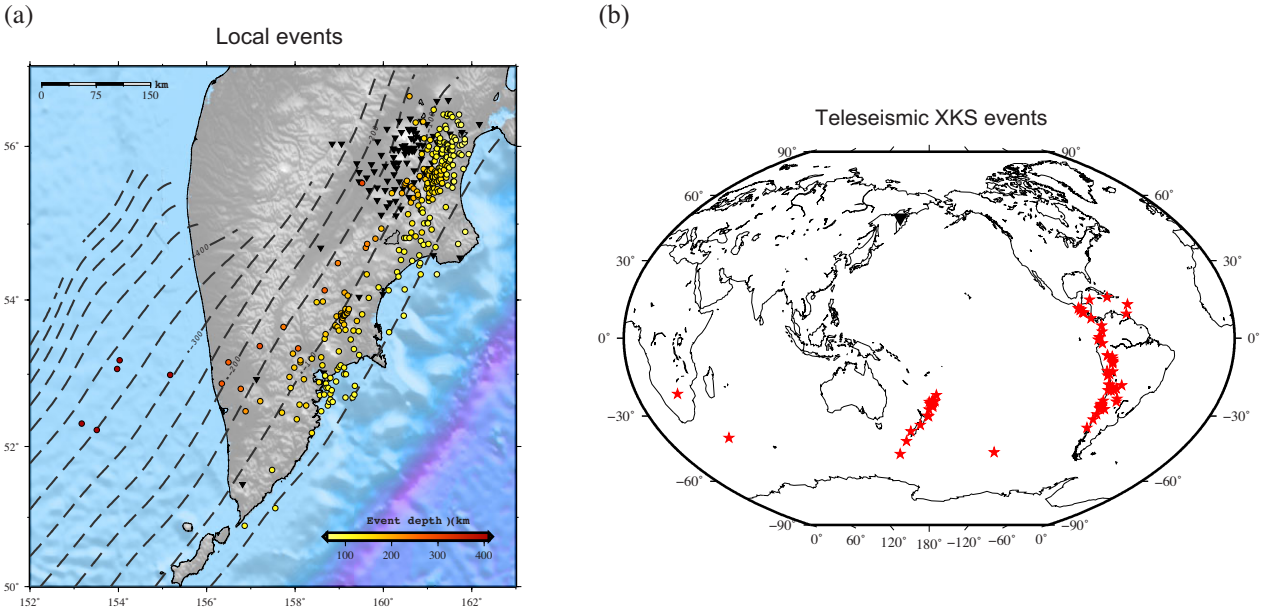

Figure 3. (a) Locations of the subduction events used for the local SWS analysis. The circles showing the events are colour-coded according to the depth of the events (yellow: shallow and red: deep). The black triangles indicate the location of the stations. (b) Locations of teleseismic events (red stars) used for the *XKS* splitting analysis. The location of the study area (Kamchatka peninsula) is indicated with a dark blue triangle.

case of a discrepancy of $> 20^{\circ}$ for the FPD or > 0.15 s for the splitting time. Following these screening criteria, we end up with 196 individual splitting measurements that are qualified as 'good' or 'fair' (Table S2, Supporting Information). We show an example of *SKS* splitting analysis in Fig. 4(b).

3 RESULTS

Processing the combined data set of both the *XKS* and local *S* provides us with the opportunity to compare the results of splitting analysis by projecting the measurements to different depths.

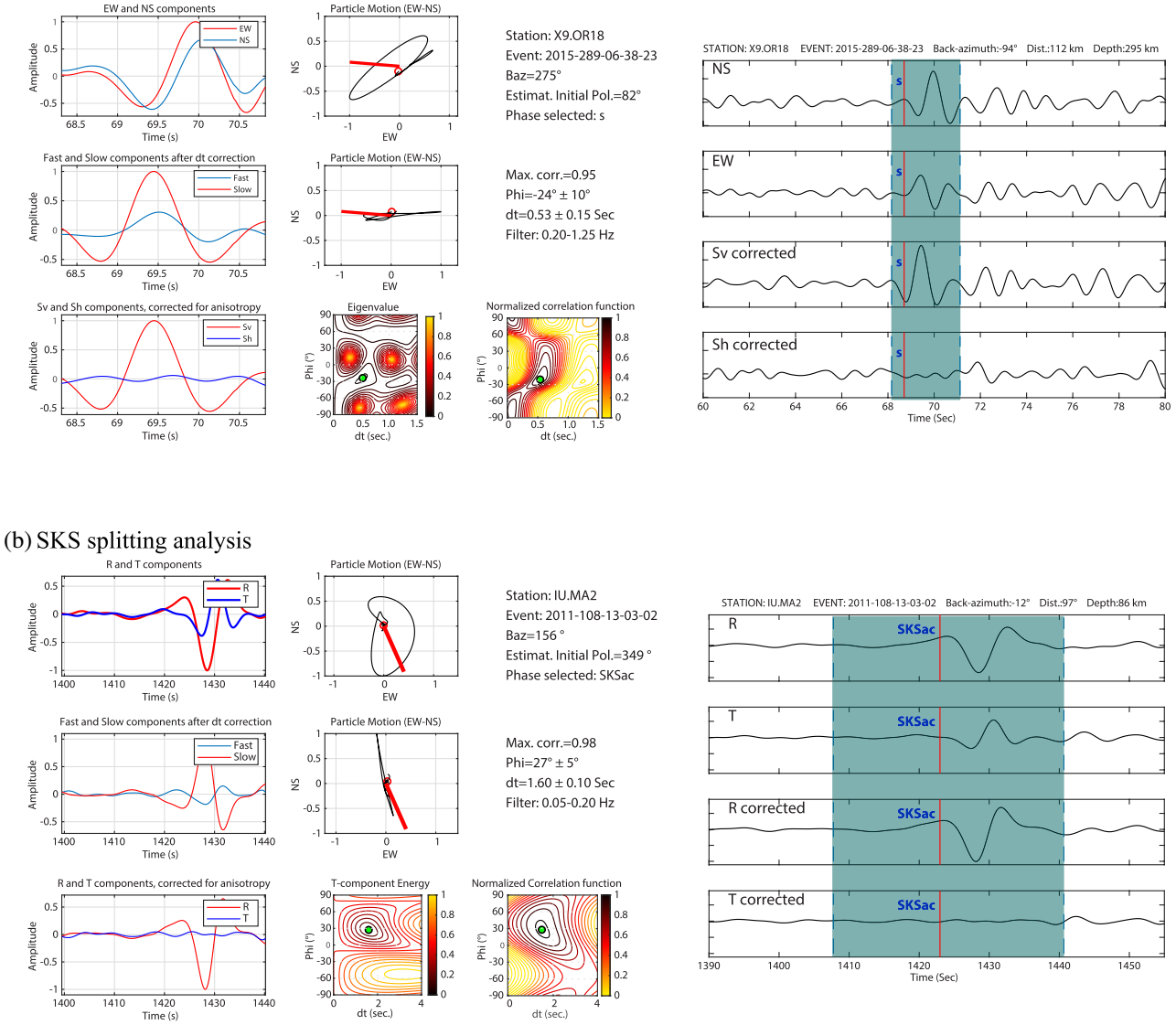

Figure 4. Examples of splitting analysis: (a) local shear and (b) SKS. In both figures, the red lines in the panels showing the particle motions indicate the geometrical backazimuth, regarding the station and event locations. For the *SKS* waves, the geometrical backazimuth should be subparallel to the polarization direction of the initial *Sv* wave before entering the anisotropic medium. For the local shear wave, the initial polarization can be a function of both backazimuth and focal mechanism of the associated event. In both sets of analysis, a cross-correlation diagram is also shown among the *T*-energy (for the *SKS* analysis) or eigenvalue (for the local *S* analysis) diagrams to compare the consistency of the splitting values obtained using two different methods. On the right-hand side, we also show the seismograms before and after corrections for anisotropy in a larger window encompassing the calculation window (the shaded zone).

3.1 *XKS* splitting results

The individual *XKS* measurements have splitting times varying between 0.1 and 2.4 s (Table S2, Supporting Information) with laterally varying FPDs. Due to the dense concentration of the seismic stations in the central volcano region (Fig. 2b), we project the individual measurements to different depths, in order to better follow the lateral variation of the *XKS* splitting measurements. In Fig. 5, we present the measurements projected to three representative depths (100, 200 and 300 km). On the left-hand side, the individual measurements are shown at the coordinates corresponding to the piercing points of the associated *XKS* ray paths at the given depth, with the red bars oriented in the FPD and with a length scaled proportionally to the corresponding splitting times. The individual measurements projected at three depths exhibit a general NW-SE trend (arcnormal/oblique) beneath the forearc region. At the single permanent station located to the NW of the study area (station IU.MA2), the individual measurements display a dominantly N-S trending FPD with an average splitting time of 1.3 s.

The measurements located beneath the KVG reveal a prevailing trend in the northeast–southwest direction, subparallel to the arc. However, due to the overlapping measurements, it becomes challenging to discern the pattern in intricate detail. Therefore, we decided to resample the measurements projected to each depth to better visualize a dominant pattern (Fig. 5, right-hand panels). For this purpose, the individual measurements are resampled over the Fresnel zone of the *XKS* wavefront at the corresponding depths by assuming a dominant period of 10 s (Alsina & Snieder 1995;

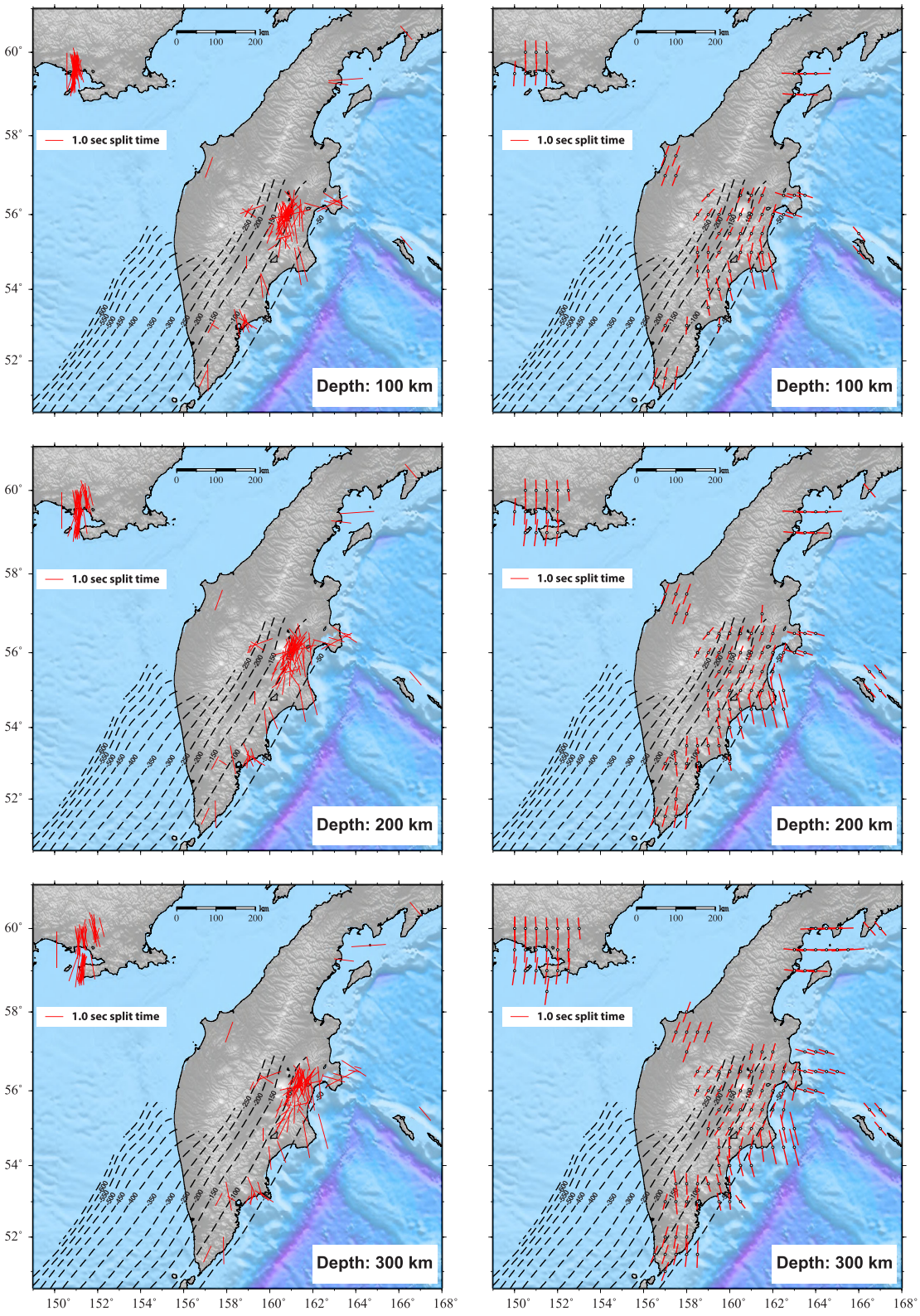

Figure 5. *XKS* splitting measurements projected to piercing points at three representative depths, 100, 200 and 300 km. The red bars are oriented in the respective FPD, with a length proportional to the associated splitting time. The left-hand panels show the individual measurements at the piercing points. The right-hand panels depict the measurements resampled over the Fresnel zone at each depth.

Rümpker & Ryberg 2000; Favier & Chevrot 2003). In the resampled maps (Fig. 5, right-hand panels), a distinct pattern of the FPDs becomes more evident. The resampled splitting measurements exhibit lateral variations, with a trend that is oblique to the trench beneath the forearc region. This trend then transitions to a predominantly arc-parallel pattern beneath the KVG, CKD and the backarc region. A few resampled points located at the western termination of the Aleutian trench show a mostly arc-parallel trend. The pattern

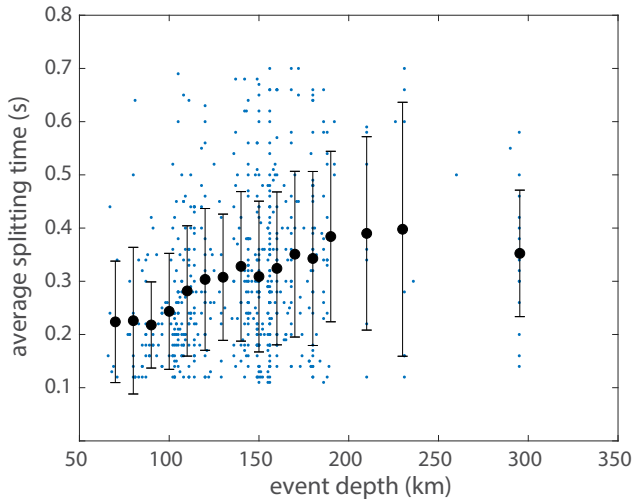

Figure 6. Average local splitting times versus event depths. Each large filled circle is the average splitting time of all measurements from events with depths of ±5 km from the target depth with the error bars indicating the standard deviation. Individual measurements are also plotted as dots in the background.

of the observed *XKS* splitting measurements indicates the potential effect of the local structure of the subducting slab on the pattern of mantle flow beneath the Kamchatka subduction zone, although there is less constraint on the exact depth where the main splitting occurs.

3.2 Local *S* splitting results

In the case of the local splitting analysis, the path (from event to station), along which the splitting occurs, is located beneath the study area. We apply a criterion of hypocentre depths of larger that 50 km to select events from the catalogue to make sure that they occur beneath the crust.

Since the majority of shallow events are located in the forearc region while our stations are located in the backarc region, regarding the constraint imposed on the incidence angle, events used for the final local splitting measurements are mostly located below the stations with depths of >75 km (Fig. 3).

We obtain relatively small local splitting times (<0.7 s, with an average of around 0.31 s), likely implying the presence of weak anisotropy in the mantle wedge. As the first indicator of the dependence of splitting times on the length of ray paths, we depict in Fig. 6 the individual (blue dots) and average (black circles with error bars) splitting times versus event depths. The average splitting time at each depth is computed using individual measurements obtained from events located within a ±5 km range of the designated depth. Despite the relatively large scatter of the individual splitting times at each depth (blue dots in Fig. 6), we observe that the average splitting time gently increases from ∼0.2 s at a depth of 50 km to ∼0.4 s at a depth of 200 km. For greater depths, the average splitting time remains nearly constant, implying that the main source of anisotropy in the mantle wedge is likely concentrated in the upper 200 km. The increase of splitting time with event depth indicates that the mantle wedge is anisotropic; nonetheless, the moderately small average splitting times imply a subtle degree of anisotropy.

A few previous studies (e.g. Kenyon & Wada 2022) report the dependence of splitting parameters on incidence angle. We also examined this dependence in our observation. Since ray paths with different incidence angles sample different regions in the mantle wedge, finding a causal link between incidence angle and splitting parameters is challenging. To reduce the effect of event depth on the values of incidence angles, we verify the variation of splitting parameters with incidence angle for events clustered at four representative depths (Fig. S1, Supporting Information). However, the scatter in the measurements does not allow us to conclude any systematic variation of the splitting parameters with incidence angle.

To examine the pattern of local splitting measurements, they are usually mapped at the location of the mid-point of the ray path (e.g. Long & Wirth 2013; Richards *et al.* 2021). We select three groups of events clustered at hypocentral depths of 100, 200 and 300 km and show the splitting measurements obtained from these events in Fig. 7. The measurements are mapped at the respective midway depths of 50, 100 and 150 km and present anisotropy in the mantle wedge. On the left-hand panels in Fig. 7, we present the individual measurements with the red bars oriented in the direction of the associated FPDs and scaled according to their splitting times. The abundant clustering of individual measurements, particularly beneath the volcanic group, makes it challenging to identify the pattern of local splitting observations. Since the splitting times are small, we focus mainly on the pattern of the FPDs and show, on the right-hand panels in Fig. 7, the FPDs colour-coded according to their orientations relative to the north. The red colour corresponds to an arc-parallel direction and the blue/green colour indicates an arc-normal/oblique direction. At all the selected projection depths (Fig. 7), we note that the FPDs from the local-*S* splitting analysis exhibit a dominantly arc-parallel orientation beneath the CKD and KVG, while it mostly displays an arc-perpendicular direction in the southwestern and eastern regions of the Kamchatka peninsula.

To further enhance the examination of lateral and vertical variations in the FPDs of local-*S* splitting within the subduction zone, we present the findings in three vertical cross-sections depicted in Fig. 8. As in Fig. 7, the FPDs are shown with colours according to their orientation relative to the north. We see clusters of the FPDs direction beneath the KVG along profiles B and C at depths 50–150 km with a dominant NE-SW (arc-parallel) orientation. On the other hand, we clearly see an arc-perpendicular/oblique orientation of anisotropy in the mantle wedge along profile A.

3.3 Comparison between the *XKS* and local-*S* splitting results

A direct comparison between the splitting results obtained from local-*S* and *XKS* waves is challenging. First, travelling on a longer ray path, *XKS* waves are dominated by longer periods (around 10 s) relative to the higher frequency (∼ 1 Hz) content of local shear waves. Previous studies (e.g. Wirth & Long 2010; Huang *et al.* 2011) have shown that splitting parameters (particularly delay time) can depend on the frequency of the shear wave used to measure splitting parameters. Secondly, the two waves take different ray paths to reach the stations. While local waves are restricted in the subduction zone beneath the seismic network, *XKS* waves travel from the core–mantle boundary to the surface. The other parameter to consider is that teleseismic waves have almost a vertical ray angle when entering the target medium beneath a subduction zone, whereas local waves may enter the anisotropic medium with a wider incidence angle. The resulting splitting measurements can be partially affected by the angle at which the *S* wave propagates into the anisotropic medium (Long and Silver, 2009). To mitigate this effect, we restrict

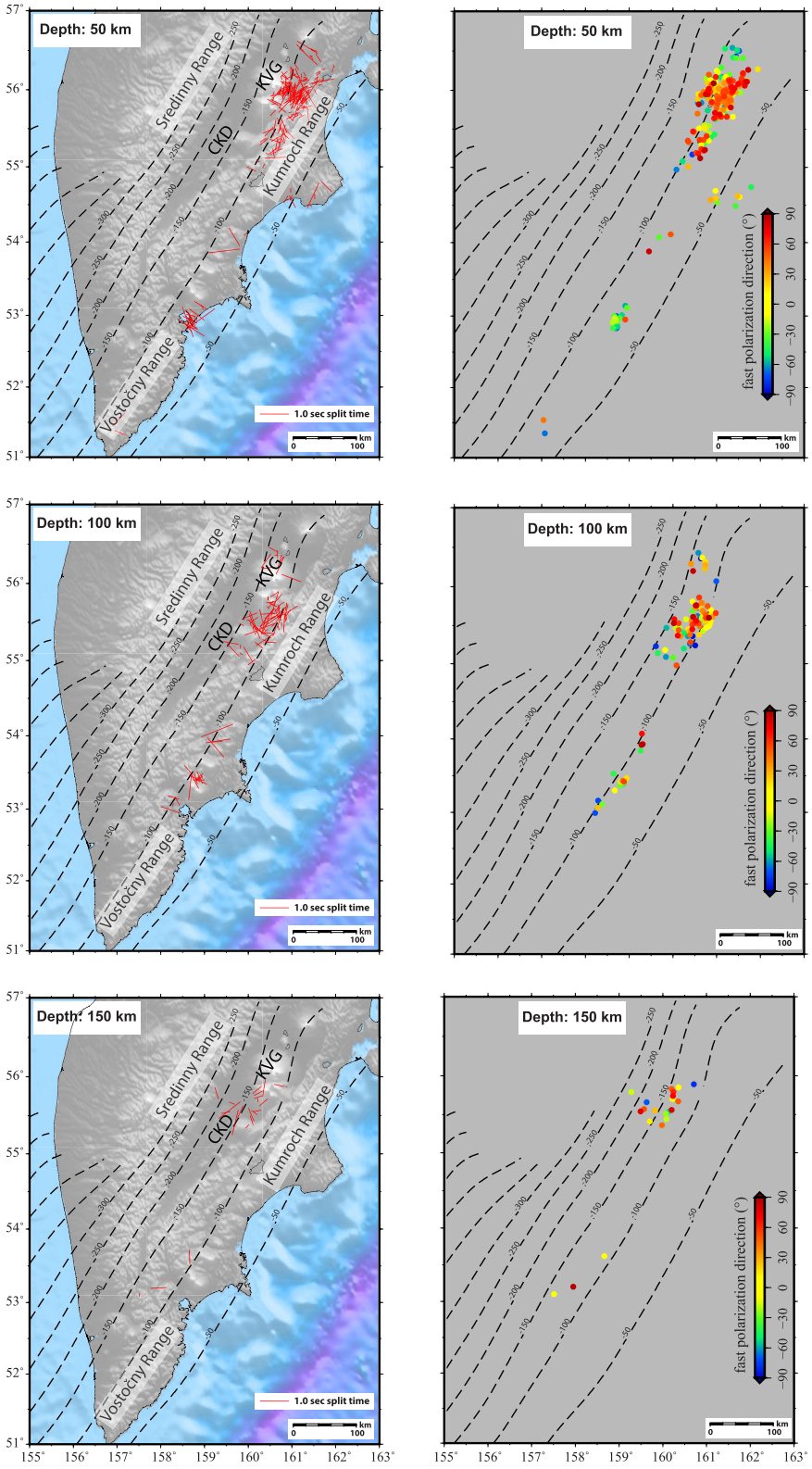

Figure 7. Local SWS results from three clusters of events occurring at depths around 100, 200 and 300 km. The splitting measurements are plotted at the location of the midway of their respective event-to-station ray paths located at depths 50, 100 and 150 km. On the left-hand side, the individual measurements are shown with red bars oriented in the FPD (φ) and with length scaled with the splitting times (δt). On the right, we present only the FPD at each point colour-scaled according to their respective orientation, with a red colour indicating an arc-parallel orientation and blue–green colour showing an arc-perpendicular/oblique orientation.

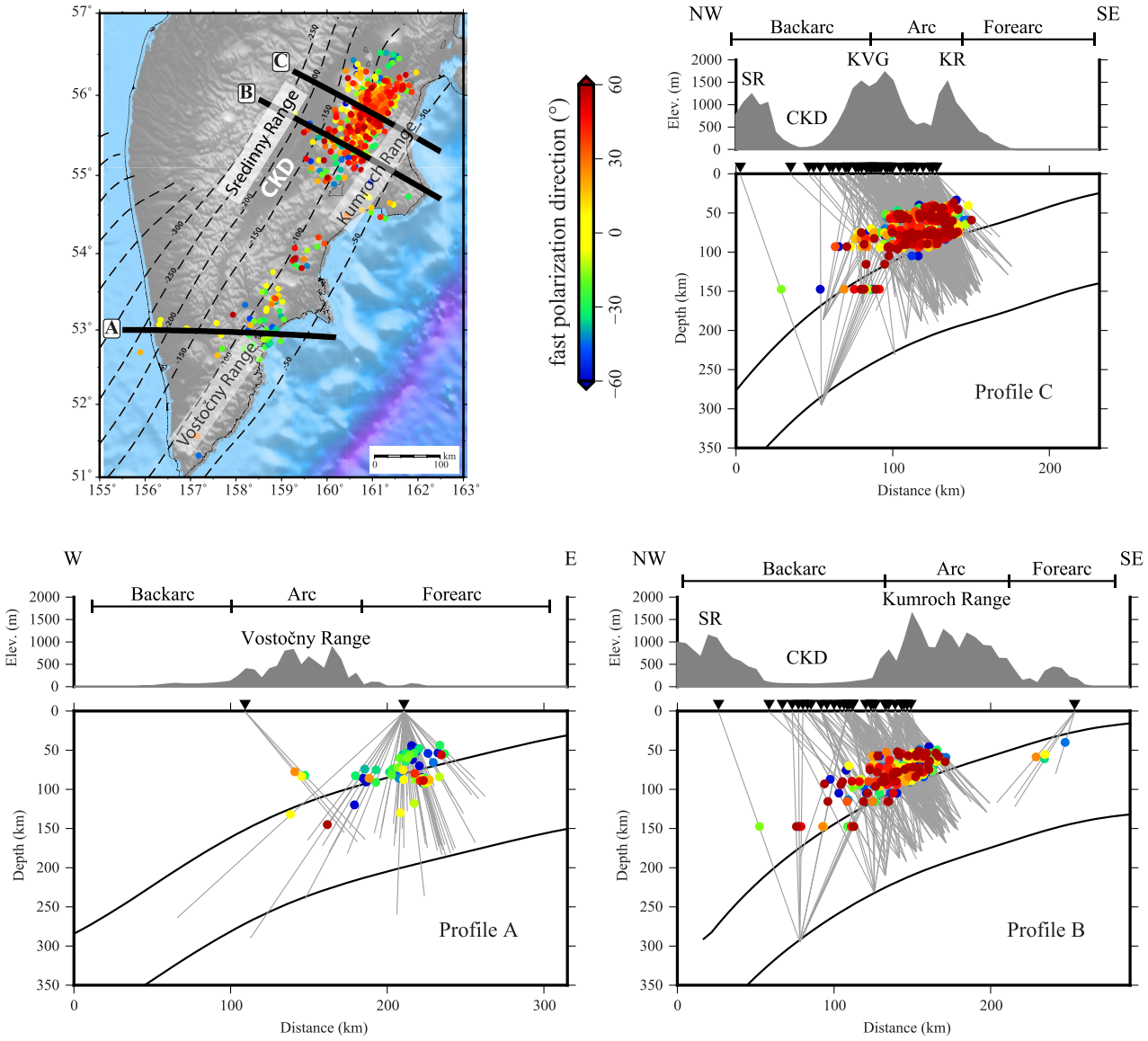

Figure 8. Vertical cross-sections showing FPDs of individual local splitting measurements. The colour scale is the same as used in Fig. 7, right-hand panel. The black triangles on the top of each profile show the location of recording along the profile. CKD: Central Kamchatka Depression; KVG: Klyuchevskoy Volcanic Group; SR: Sredinny Range; KR: Kumroch Range and TR: Tumrok Range.

the incidence angle of local shear waves to be less than 35°. Furthermore, as we resample the individual measurements over the Fresnel volume, the effect of differing ray angles is partially reduced. We are, however, aware that local-*S* splitting measurements are more sensitive to short-scale variations in anisotropic structure relative to *XKS* waves.

In order to gain insight into the possible sources of anisotropy in the mantle, we compare (Fig. 9) the *XKS* and local-*S* splitting results projected to four depths (50, 75, 100 and 150 km). This comparison provides primary clues about the depth variation of anisotropy. The pattern of the resampled splitting measurements is shown at the respective depths with red bars indicating the resampled local-*S* splitting and yellow bars indicating the resampled *XKS* splitting, all shown at the same scale, proportional to their respective splitting times. The main purpose of this comparison is to examine the consistency between the *XKS* and local-*S* splitting observations assuming that they both occur at the same depth. The local-*S* observations can better represent anisotropy at the respective depth, however, there is much less constraint on the depth at which the *XKS* splitting occurs. At all depths, we observe a relatively good agreement between the patterns of the FPDs obtained from the two observations. The FPDs are dominantly arc-parallel beneath the CKD and KVG, whereas they become mainly arc-perpendicular/oblique in the forearc region. The lateral variation of the local-*S* FPDs can be the result of short-scale local deformation in the mantle wedge, which has less effect on the *XKS* measurements due to sampling over a larger Fresnel volume. On the other hand, the larger splitting times of the *XKS* measurements relative to those of the local *S* imply that besides the mantle wedge, the deeper mantle including the subducting slab and subslab mantle may also be involved in the splitting of the *XKS* waves. The consistency between the patterns of FPDs from both data sets, despite the difference in splitting times, implies a consistency of the pattern of anisotropy in the mantle wedge and subslab mantle beneath the CKD.

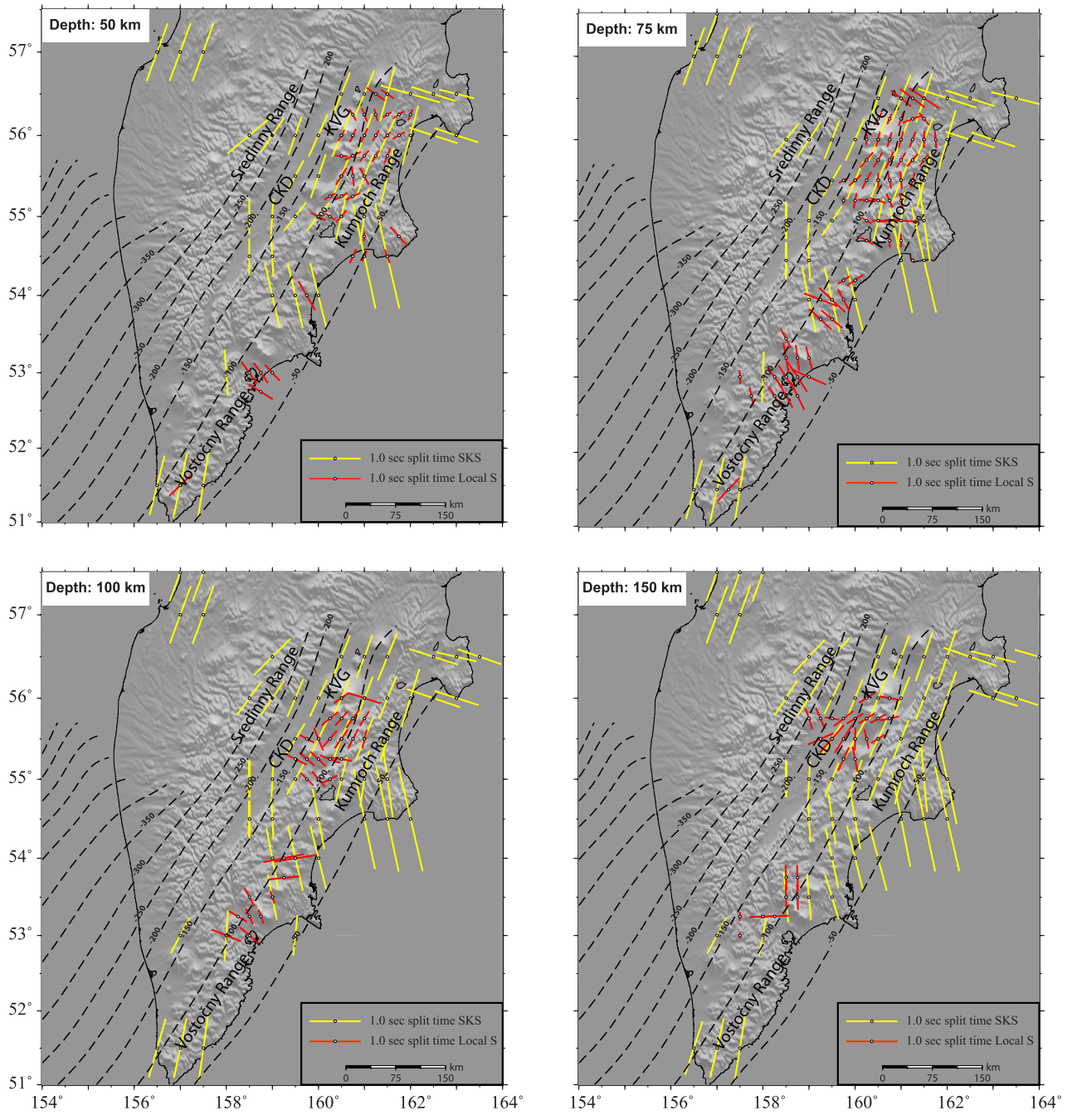

Figure 9. A comparison between the local-*S* and *XKS* splitting measurements projected at four representative depths 50, 75, 100 and 150 km. The individual measurements are resampled over the Fresnel zone at the respective depths, assuming 2 and 10 s of dominant periods for the local-*S* and *XKS* waves, respectively. Red and yellow bars show the local-*S* and *XKS* splitting measurements, respectively, with the length proportional to their splitting time. The local-*S* measurements are plotted at the midway of the ray paths from event to station. The *XKS* measurements are projected at the piercing points of the respective rays at each depth.

4 DISCUSSION

The splitting analysis of both local (subduction) and teleseismic (*XKS*) shear waves can provide better constraints to examine the depth of the source of anisotropy in subduction zones (e.g. Long & Silver 2008; Long & Wirth 2013; Wölbern *et al.* 2014; Reiss *et al.* 2018). While fewer constraints exist on the depth where the main part of splitting on *XKS* waves occurs, splitting of local shear waves primarily arises from anisotropy in the mantle wedge. Therefore, the level of correlation between the two sets of measurements is a crucial indicator of the distribution of anisotropy and the flow pattern beneath a subduction zone. We present the results of the splitting analysis of shear waves from both local events and *XKS* phases to examine the pattern of mantle flow beneath the NE ending of the KSZ. We discuss our findings within the tectonic context of the KSZ, taking into account the correlation between the splitting measurements obtained from the two sets of data. At a large scale, we observe consistency between the pattern of the local shear and *XKS*

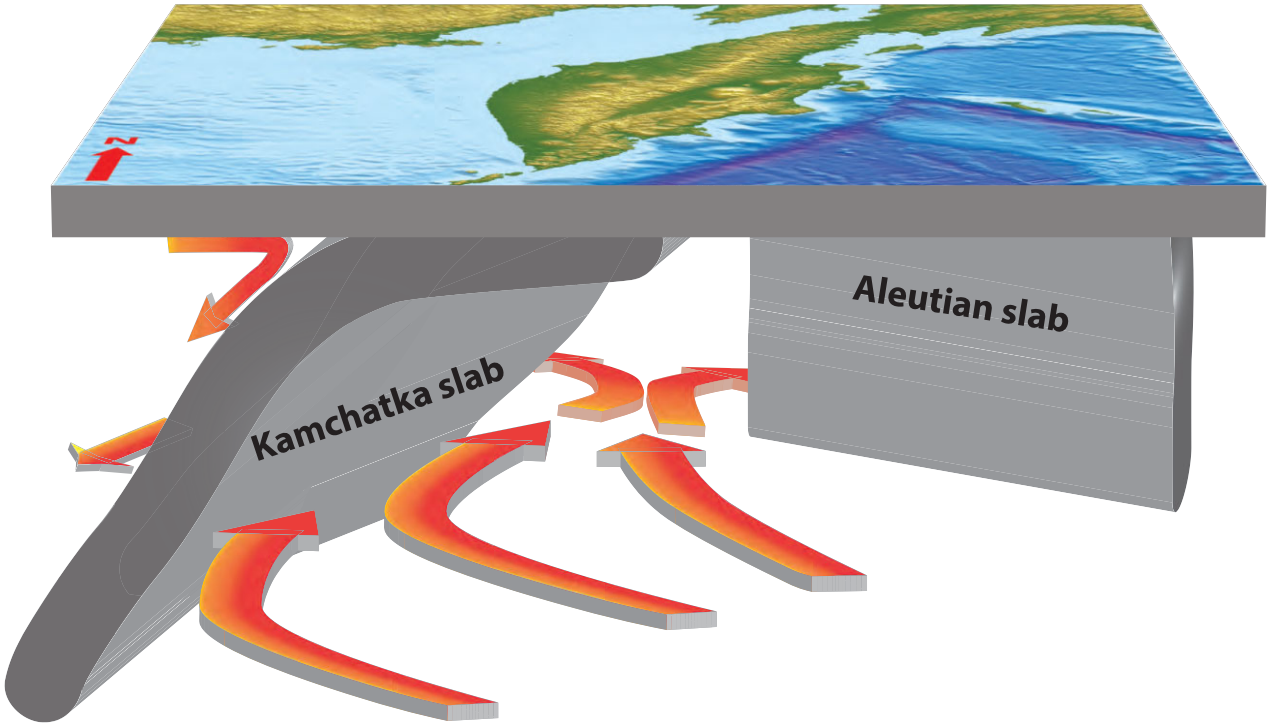

Figure 10. A 3-D sketch view of the suggested pattern of mantle flow beneath the study area. The flow developed by lithospheric drag diverges into the existing window at the termination of the two slabs. The encounter of the flow with the edge of the Kamchatka slab can create a toroidal pattern.

splitting observations (Fig. 9). Both sets of observations show arc-parallel fast directions beneath the CKD and specifically under the KVG, and a dominantly arc-perpendicular or arc-oblique direction in the forearc region along the eastern coast of the Kamchatka Peninsula.

4.1 Mantle wedge anisotropy

The small splitting times from local shear wave analyses (Figs 6 and 7), which were also reported by previous studies (Levin *et al.* 2004), suggest the presence of weak and heterogeneous anisotropy in the mantle wedge beneath Kamchatka.

Lynner & Long (2014) investigated source-side anisotropy globally under subduction zones. Their findings show fast directions that are mainly subparallel to the direction of slab motion beneath the northern Kurile, south of the Kamchatka Peninsula. These directions are comparable to the trench-normal directions that we find in southern Kamchatka. These observations support the idea that anisotropy in the subslab mantle is related to the large-scale Plate-Motion-parallel flow and also imply that a trench-normal 2-D flow is the dominant mechanism in the mantle wedge away from the slab edge to the north.

Reiss *et al.* (2018) also observed that the mantle wedge in the forearc region of the central Andean margin has a negligible contribution to SWS observation. Despite the small-scale lateral variation of the FPDs and small splitting times, we observe a dominant pattern of local splitting observations with an arc-perpendicular trend beneath the arc regions and an arc-parallel trend beneath the CKD and KVG (Figs 7 and 8). This pattern contradicts the observations made at numerous other subduction zones globally (e.g. Hall *et al.* 2000; León Soto *et al.* 2009; Long & Wirdth 2013; Kong *et al.* 2020; Richards *et al.* 2021), where the fast directions are reported to be dominantly arc parallel in arc and forearc regions and arc perpendicular in backarc regions. The arc-perpendicular anisotropy in backarc regions is often interpreted as indicative of 2-D corner flow in the mantle wedge, whereas the arc-parallel fast directions in forearc regions are attributed to B-type LPO fabric that is also generated by the corner flow in the colder and hydrated portion of the mantle wedge (Kneller *et al.* 2005; Karato *et al.* 2008). However, flow in the mantle wedge can be affected by other parameters such as oblique subduction, slab geometry and slab termination (e.g. Honda & Yoshida 2005; Kneller & van Keken 2008; MacDougall *et al.* 2014; Kenyon & Wada 2022). The geometry of the slab beneath the Kamchatka Peninsula may hamper the development of a large-scale uniform anisotropy in the mantle wedge. The presence of undeformed hydrous minerals such as antigorite could also be a cause of weak anisotropy in the mantle wedge (Jung 2011; Horn *et al.* 2020). Arc-perpendicular anisotropy in the mangle wedge from our local splitting analysis can be due to the 2-D corner flow for the regions away from the CKD. In addition, the presence of fossil LPO fabric in the subducting Pacific plate can also generate arc-perpendicular FPDs as was also suggested for south-central Alaska (Karlowska *et al.* 2021). The observation of arc-parallel FPDs from the mantle wedge in the backarc region beneath the CKD, where a hot and anhydrous condition is expected (Koulakov *et al.* 2020), requires the presence of persisting flow with an arc-parallel component rather than a B-type LPO fabric to explain the observations. We further discuss this pattern in correlation with the arc-parallel FPDs also observed from the *XKS* splitting analysis.

4.2 Rotational flow at the slab edge

The most significant striking finding in our study is the observation of the rotational pattern of the fast directions from a dominantly

arc-perpendicular trend beneath the arc and forearc regions to a prevailing arc-parallel trend beneath the CKD and KVG, observed both by the local shear and *XKS* waves. The rotational pattern of anisotropy beneath the CKD implies that a toroidal flow is likely developing at the NE edge of the slab as it was also suggested by previous seismic anisotropy studies (Peyton *et al.* 2001; Levin *et al.* 2004). For the regions beyond the slab edge beneath the forearc region, the subslab mantle flow is mainly governed by the drag of the Pacific plate over the underlying asthenosphere generating arc-perpendicular LPO. Fig. 10 schematically illustrates the inferred pattern of subslab flow that diverges parallel to the trench to enter the window between the two slabs: Kamchatka slab in the south and Aleutian slab to the north. Using surface-wave azimuthal anisotropy tomography, Zhao *et al.* (2021) also report evidence for the toroidal mantle flow at the slab edge beneath Kamchatka. Other seismic tomography studies (Koulakov *et al.* 2011; 2020) also suggest the termination of the slab beneath the NE of the Kamchatka Peninsula. These studies also reveal the signature of the upward flow of material from the deep mantle into the mantle wedge through the slab window. This upward flow serves as the main source for the vast volcanism in the region (Koulakov *et al.* 2020) and can also have effects on the dynamic uplift of the over-riding plate (e.g. Király *et al.* 2020). The toroidal flow pattern at the slab edge was also observed in other subduction zones (e.g. León Soto *et al.* 2009; Long & Wirdth 2013; Kong *et al.* 2020). Geodynamic modelling studies (e.g. Faccenda & Capitanio 2013) suggest that toroidal flow with a dominant horizontal component can develop near the lateral edges of the slab. The correlation between the *XKS* and local-*S* splitting patterns suggests that XKS waves are also affected by anisotropy in the mantle wedge. On the other hand, the small splitting times from the local splitting measurements imply that the coherent anisotropy in the mantle wedge is relatively weak. Therefore, a main part of the *XKS* splitting might occur in the subslab mantle from a pattern of anisotropy that is consistent with the dominant anisotropy in the mantle wedge. This implies that the arc-parallel flow field in the mantle wedge beneath the KVG is subparallel with the flow in the subslab mantle. We argue that the toroidal flow at the slab edge produces an arc-parallel component both atop and underneath the slab.

We propose that the gap between the Kamchatka and Aleutian slabs in the NE of the Kamchatka peninsula not only serves as a source wellspring for the prevalent active volcanic activity in the area but also plays a significant role in the dynamics of regional tectonics.

5 CONCLUSION

The splitting analysis of shear waves from local (subduction) events and teleseismic core-refracted shear waves (*XKS* family) from a dense network of seismic stations allow us to investigate seismic anisotropy beneath the NE termination of the KSZ in the Kamchatka peninsula. We obtained splitting parameters from local shear waves at 99 broad-band and short-period stations. For the *XKS* splitting analysis, we only used data from 69 broad-band stations. The combined data sets allowed us to intuitively examine the depth distribution of anisotropy. Through examining the characteristics of seismic anisotropy, we have derived several key findings pertaining to the flow patterns within the mantle wedge and subslab mantle beneath the Kamchatka peninsula.

Local shear waves exhibit relatively small splitting times with lateral variation in the fast directions suggesting the existence of weak and somewhat variable anisotropy within the mantle wedge. However, in general, both the *XKS* and local-*S* splitting measurements indicate arc-parallel fast directions beneath the volcanic group of central Kamchatka. In contrast, the arc region along the eastern border of the peninsula exhibits arc-perpendicular (or arc-oblique) fast directions.

The observed lateral variation of fast axes in the local-*S* splitting data dismisses the possibility of a straightforward 2-D corner flow model within the mantle wedge beneath the Kamchatka subduction zone. The overall agreement between the local-*S* and *XKS* splitting patterns, which exhibit a clockwise rotation beneath the CKD, suggests the presence of a toroidal flow at the northeastern edge of the Kuril slab. The gap between the Kuril and Aleutian slabs in the NE of the Kamchatka peninsula facilitates the divergence of the subslab flow along the strike. The entrance of flow from both sides into the slab window can cause a turbulent pattern. This flow likely influences both the mantle wedge and the subslab mantle.

ACKNOWLEDGMENTS

We are thankful to GFZ Data Services and the GEOFON program for providing the waveform data from the KISS experiment. The IRIS Data Management Center is also acknowledged for the data from previous temporary deployments and the two permanent stations used in this study.

We are also grateful of Dr Xiaobo He and an anonymous reviewer for their constructive comments that helped us improve the content and conclusions of the manuscript.

DATA AVAILABILITY

Waveform data from the KISS experiment are publically available through the GFZ Data Services and the GEOFON program. Data from previous temporary deployments and the two permanent stations used in this study are also accessible via the IRIS Data Management Center. The origin time and location of local events were downloaded from the website of the Kamchatka Branch of the Geophysical Survey of the Russian Academy of Sciences (Chebrov *et al.* 2013, 2020; http://sdis.emsd.ru/info/earthquakes/catalogue.php). We also included the local events from the catalogue recently published by Senyukov et al. (2023) based on the data set from the KISS experiment for the duration of deployments.

CONFLICT OF INTEREST

We confirm that there are no conflicts of interest for all authors in any part of this research (including funding and data set).

SUPPORTING INFORMATION

Supplementary data are available at *GJI* online.

Fig. S1. Presentation of splitting parameters versus incidence angles for measurements from four cluster of events occurred at depths around 60, 100, 140 and 180 km.

Table S1. Individual measurements obtained from local SWS analysis (see the accompanying Excel file: Local_splitting_results_Kamchatka).

Table S2. Individual measurements obtained from *XKS* splitting analysis (see the accompanying Excel file: SKS_splitting_results_Kamchatka).

Please note: Oxford University Press are not responsible for the content or functionality of any supporting materials supplied by the authors. Any queries (other than missing material) should be directed to the corresponding author for the article.

FUNDING

AK benefited from funding supported by the German Research Foundation (DFG) under the grant number: RU 886/16-1.

REFERENCES

Alsina, D. & Snieder, R., 1995. Small-scale sublithospheric continental mantle deformation: constraints from SKS splitting observations, *Geophys. J. Int.,* **123,** 431–448.

Ben Ismail, W. & Mainprice, D., 1998. An olivine fabric database: an overview of upper mantle fabrics and seismic anisotropy, *Tectonophysics,* **296,** 145–157.

Bowman, J.R. & Ando, M., 1987. Shear-wave splitting in the upper-mantle wedge above the Tonga subduction zone, *Geophys. J. R. astron. Soc.,* **88,** 25–41.

Chebrov, V.N., Droznin, D.V., Kugaenko, Y.A., Levina, V.I., Senyukov, S.L., Sergeev, V.A., Shevchenko, Y.V. & Yashchuk, V.V., 2013. The system of detailed seismological observations in Kamchatka in 2011, *J. Volc. Seismol.,* **7,** 16–36.

Chebrova, A.Y.., Chemarev, A.S., Matveenko, E.A. & Chebrov, D.V., 2020. Seismological data information system in Kamchatka branch of GS RAS: organization principles, main elements and key functions, *Geophys. Res.,* **21,** 66–91.

Faccenda, M. & Capitanio, F.A., 2013. Seismic anisotropy around subduction zones: insights from three-dimensional modeling of upper mantle deformation and SKS splitting calculations, *Geochem. Geophys. Geosyst.,* **14,** 243–262.

Favier, N. & Chevrot, S., 2003. Sensitivity kernels for shear wave splitting in transverse isotropic media, *Geophys. J. Int.,* **153,** 213–228.

Fedotov, S., Zharinov, N. & Gontovaya, L., 2010. The magmatic system of the Klyuchevskaya group of volcanoes inferred from data on its eruptions, earthquakes, deformation & deep structure, *J. Volc. Seismolog.,* **4**(1), 1–33.

Hall, C.E., Fischer, K.M., Parmentier, E.M. & Blackman, D.K., 2000. The influence of plate motions on three-dimensional back arc mantle flow and shear wave splitting, *J. geophys. Res.,* **105,** 28009–28033.

Hayes, G., 2018. Slab2–a comprehensive Subduction zone geometry model, *U.S. Geological Survey data release,* doi: 10.5066/F7PV6JNV.

Honda, S. & Yoshida, T., 2005. Effects of oblique subduction on the 3-D pattern of small-scale convection within the mantle wedge, *Geophys. Res. Lett.,* **32,** L13307, doi:10.1029/2005GL023106.

Horn, C., Bouilhol, P. & Skemer, P., 2020. Serpentinization, deformation & seismic anisotropy in the subduction mantle wedge, *Geochem. Geophys. Geosyst.,* **21,** e2020GC008950, doi:10.1029/2020GC008950.

Huang, Z., Zhao, D. & Wang, L., 2011. Frequency-dependent shear-wave splitting and multilayer anisotropy in northeast Japan, *Geophys. Res. Lett.,* **38,** doi:10.1029/2011GL046804.

Jung, H., 2011. Seismic anisotropy produced by serpentine in mantle wedge, *Earth planet. Sci. Lett.,* **307,** 535–543.

Karato, S.-i., Jung, H., Katayama, I. & Skemer, P., 2008. Geodynamic significance of seismic anisotropy of the upper mantle: new insights from laboratory studies, *Annu. Rev. Earth Planet. Sci.,* **36,** 59–95.

Karlowska, E., Bastow, I.D., Rondenay, S., Martin-Short, R. & Allen, R.M., 2021. The development of seismic anisotropy below south-central Alaska: evidence from local earthquake shear wave splitting, *Geophys. J. Int.,* **225,** 548–554.

Kaviani, A., Hofstetter, R., Rümpker, G. & Weber, M., 2013. Investigation of seismic anisotropy beneath the Dead Sea fault using dense networks of broadband stations, *J. geophys. Res. Solid Earth,* **118,** 3476–3491.

Kenyon, L.M. & Wada, I., 2022. Mantle wedge seismic anisotropy and shear wave splitting: effects of oblique subduction, *J. geophys. Res.: Solid Earth,* **127,** e2021JB022752. doi: 10.1029/2021JB022752.

Király, A. *et al.*, 2020. The effect of slab gaps on subduction dynamics and mantle upwelling, *Tectonophysics,* **785,** 228458. doi:10.1016/j.tecto.2020.228458.

Kneller, E.A. & van Keken, P.E., 2008. Effect of three-dimensional slab geometry on deformation in the mantle wedge: implications for shear wave anisotropy, *Geochem. Geophys. Geosyst.,* **9,** Q01003, doi:10.1029/2007GC001677.

Kneller, E.A., van Keken, P.E., Karato, S.-i. & Park, J., 2005. B-type olivine fabric in the mantle wedge: insights from high-resolution non-Newtonian subduction zone models, *Earth planet. Sci. Lett.,* **237,** 781–797.

Kong, F., Gao, S.S., Liu, K.H., Zhang, J. & Li, J., 2020. Seismic anisotropy and mantle flow in the Sumatra subduction zone constrained by shear wave splitting and receiver function analyses, *Geochem. Geophys. Geosyst.,* **21,** e2019GC008766. doi:10.1029/2019GC008766.

Koulakov, I. *et al.*, 2020. Mantle and crustal sources of magmatic activity of Klyuchevskoy and surrounding volcanoes in Kamchatka inferred from earthquake tomography, *J. geophys. Res.: Solid Earth,* **125,** e2020JB020097. doi:10.1029/2020JB020097.

Koulakov, I.Y., 2022. Seismic tomography of Kamchatkan Volcanoes, *Russ. Geol. Geophys.,* **63**(11), 1207–1244.

Koulakov, I.Y., Dobretsov, N.L., Bushenkova, N.A. & Yakovlev, A.V., 2011. Slab shape in subduction zones beneath the Kurile-Kamchatka and Aleutian arcs based on regional tomography results, *Russ. Geol. Geophys.,* **52**(6), 650–667.

Kreemer, C., Blewitt, G. & Klein, E.C., 2014. A geodetic plate motion and global strain rate model, *Geochem. Geophys. Geosyst.,* **15**(10), 3849–3889.

León Soto, G. *et al.*, 2009. Mantle flow in the Rivera—Cocos subduction zone, *Geophys. J. Int.,* **179,** 1004–1012.

Levin, V. *et al.*, 2004. Detailed mapping of seismic anisotropy with local shear waves in southeastern Kamchatka, *Geophys. J. Int.,* **158,** 1009–1023.

Levin, V. *et al.*, 2002. Seismic evidence for catastrophic slab loss beneath Kamchatka, *Nature,* **418,** 763–767.

Long, M.D., 2013. Constraints on subduction geodynamics from seismic anisotropy, *Rev. Geophys.,* **51,** 76–112.

Long, M.D. & Silver, P.G., 2008. The subduction zone flow field from seismic anisotropy: a global view, *Science,* **319**(5861), 315–318.

Long, M.D. & Silver, P.G., 2009. Mantle flow in subduction systems: the subslab flow field and implications for mantle dynamics, *J. geophys. Res.,* **114,** B10312. doi:10.1029/2008JB006200.

Long, M.D. & Wirth, E.A., 2013. Mantle flow in subduction systems: the mantle wedge flow field and implications for wedge processes, *J. geophys. Res.,* **118,** 583–606.

Lynner, C. & Long, M.D., 2014. Sub-slab anisotropy beneath the Sumatra and circum-Pacific subduction zones from source-side shear wave splitting observations, *Geochem. Geophys. Geosyst.,* **15,** 2262–2281.

MacDougall, J.G., Kincaid, C., Szwaja, S. & Fischer, K.M., 2014. The impact of slab dip variations, gaps and rollback on mantle wedge flow: insights from fluids experiments, *Geophys. J. Int.,* **197,** 705–730.

Peyton, V., Levin, V., Park, J., Brandon, M., Lees, J., Gordeev, E. & Ozerov, A., 2001. Mantle flow at a slab edge: seismic anisotropy in the Kamchatka region, *Geophys. Res. Lett.,* **28**(2), 379–382.

Ponomareva, V.V. *et al.*, (eds), 2007. *Volcanism and Subduction: The Kamchatka Region, AGU Geophysical Monograph Series,* Vol., **172,** pp. 165–198. American Geophysical Union.

Portnyagin, M., Hoernle, K., Avdeiko, G., Hauff, F., Werner, R., Bindeman, I., Uspensky, V. & Garbe-Schönberg, D., 2005. Transition from arc to oceanic magmatism at the Kamchatka-aleutian junction, *Geology,* **33**(1), 25–28.

Reiss, M.C. & Rümpker, G., 2017. SplitRacer: MATLAB code and GUI for semiautomated analysis and interpretation of teleseismic shear-wave splitting, *Seismol. Res. Lett.,* **88**(2A), 392–409.

Reiss, M.C., Rümpker, G. & Wölbern, I., 2018. Large-scale arc-perpendicular mantle flow beneath central South America, *Earth planet. Sci. Lett.,* **482,** 115–125,.

Richards, C., Tape, C., Abers, G.A. & Ross, Z.E., 2021. Anisotropy variations in the Alaska subduction zone based on shear-wave splitting from intraslab earthquakes, *Geochem. Geophys. Geosyst.,* **22,** e2020GC009558. doi:10.1029/2020GC009558.

Rümpker, G. & Ryberg, T., 2000. New "Fresnel-zone" estimates for shear-wave splitting observations from finite-difference modeling, *Geophys. Res. Lett.,* **27**(13), 2005–2008.

Savage, M.K., 1999. Seismic anisotropy and mantle deformation: what have we learned from shear wave splitting?, *Rev. Geophys.,* **37,** 65–106.

Senyukov, S., 2013. Monitoring and prediction of volcanic activity in Kamchatka from seismological data: 2000–2010, *J. Volc. Seismolog.,* **7**(1), 86–97.

Senyukov, S.L., Droznin, D.V., Droznina, S.Y., Shapiro, N.M. & Nuzhdina, I.N., 2024. The KISS Network in 2015–2016: Catalogs and Comparison of the Processing Results with Operational Estimates from the Permanent Network (in Russian), *Izv., Phys. Solid Earth,* **2,** 146–160.

Senyukov, S.L., Nuzhdina, I.N., Droznina, S.Y., Garbuzova, V.T., Kozhevnikova, T.Y., Sobolevskaya, O.V., Nazarova, Z.A. & Bliznetsov, V.E., 2015. Seismic monitoring of the Plosky Tolbachik eruption in 2012–2013, Kamchatka Peninsula Russia, *J. Volc. Geotherm. Res.,* **302,** 117–159.

Shapiro, N.M. *et al.*, 2017. Understanding Kamchatka's extraordinary volcano cluster, *Eos,* **98**(7), 12–17.

Shapiro, N.M. *et al.*, 2021. Klyuchevskoy volcanic group experiment (KISS): supplementary data of the passive seismological measurement, *GFZ Data Services,* doi: 10.5880/GIPP.201505.1.

Silver, P.G., 1996. Seismic anisotropy beneath the continents, probing the depths of geology, *Ann. Rev. Earth planet. Sci.,* **24,** 385–432.

Silver, P.G. & Chan, W.W., 1991. Shear wave splitting and subcontinental mantle deformation, *J. geophys. Res.,* **96,** 16429–16454.

Silver, P.G. & Savage, M.K., 1994. The interpretation of shear-wave splitting parameters in the presence of two anisotropic layers, *Geophys. J. Int.,* **119**(3), 949–963.

Steblov, G.M. *et al.*, 2010. Dynamics of the Kuril-Kamchatka subduction zone from GPS data, *Izv., Phys. Solid Earth,* **46,** 440–445.

van Keken, P.E., 2003. The structure and dynamics of the mantle wedge, *Earth planet. Sci. Lett.,* **215**(3), 323–338.

Wirth, E. & Long, M.D., 2010. Frequency-dependent shear wave splitting beneath the Japan and Izu-Bonin subduction zones, *Phys. Earth planet. Inter.,* **181,** 141–154.

Wölbern, I., Löbl, U. & Rümpker, G., 2014. Crustal origin of arc-parallel shear wave fast polarizations in the Central Andes, *Earth planet. Sci. Lett.,* **392,** 230–238.

Zhang, S. & Karato, S., 1995. Lattice preferred orientation of olivine aggregates deformed in simple shear, *Nature,* **375,** 774–777.

Zhao, D., Liu, X., Wang, Z. & Gou, T., 2023. Seismic anisotropy tomography and mantle dynamics, *Surv. Geophys,* **44,** 947–982.

Zhao, L., Liu, X., Zhao, D., Wang, X. & Qiao, Q., 2021. Mapping the Pacific slab edge and toroidal mantle flow beneath Kamchatka, *J. geophys. Res.: Solid Earth,* **126,** e2021JB022518. doi:10.1029/2021JB022518.